Electronic Supplementary Material (ESI) for Green Chemistry.
This journal is © The Royal Society of Chemistry 2023

Electronic Supporting Information

A Highly Active, Thermally Robust Iron(III)/Potassium(I) Heterodinuclear Catalyst for Bio-derived Epoxide/Anhydride Ring Opening Copolymerizations

Wilfred T. Diment, Gloria Rosetto, Noura Ezaz-Nikpay, Ryan W. F. Kerr and Charlotte K. Williams*

Chemistry Research Laboratory, Department of Chemistry, University of Oxford, 12 Mansfield Road, Oxford, OX1 3TA, UK.

General Procedures and Materials

All synthetic manipulations were carried out in a nitrogen filled glovebox, or a dual manifold nitrogen-vacuum Schlenk line. Solvents used in synthesis were collected from a solvent purification system (SPS), degassed with three freeze-pump-thaw cycles and stored over 3 Å molecular sieves under an inert atmosphere, unless otherwise stated. 2-MeTHF was purchased from Sigma Aldrich, degassed, and stored over molecular sieves. All materials were stored under a nitrogen atmosphere, in a glovebox. Iron(II) acetate (95%) and potassium acetate were purchased from Sigma Aldrich and was used as received.

Cyclohexene oxide (CHO, Acros Organics) and limonene oxide (LO, Sigma Aldrich) were purified by stirring over calcium hydride followed by fractional distillation. Menth-2-ene oxide (MO) was synthesised following a literature procedure, and was purified by stirring over calcium hydride, followed by fractional distillation.[1] Phthalic anhydride (PA, Sigma Aldrich) was purified though a three-step procedure. Firstly, PA was stirred in dry toluene, at room temperature, for 16 hours. The supernatant was filtered, and the toluene subsequently removed *in vacuo*. The resultant white powder recrystallised from hot (60 °C) chloroform and subsequently sublimed under vacuum at 80 °C. Camphoric anhydride (Sigma Aldrich) was purified by recrystallisation from ethyl acetate, followed by sublimation under high vacuum at 80 °C. Tricyclic anhydride was synthesised following a literature procedure and was purified by recrystallisation from hexane, followed by sublimation under high vacuum at 80 °C.[2] Furan anhydride was synthesised following a literature procedure and was purified by recrystallisation from ethyl acetate followed by sublimation under high vacuum at 80 °C.[3] The pro-ligand, [$L_{van}H_2$], was synthesised following a literature procedure.[4]

Methods

NMR Spectroscopy: ^{1}H NMR spectra were obtained using a Bruker Avance III HD 400 NMR spectrometer.

IR Spectroscopy: Carried out on a Shimadzu IR-Spirit FT-IR spectrometer equipped with a single reflection ATR (attenuated total reflectance) accessory, in a nitrogen filled glovebox.

Superconducting Quantum Interference Device (SQUID) Magnetometry: Measurements were carried out on powdered samples using a Quantum Design MPMS-3 Magnetometer, with a field of 0.1 T, at temperatures of 2 - 300 K. All magnetic susceptibility values were corrected using the diamagnetic Pascal constants.

GPC analysis: Carried out using a Shimadzu LC-20AD instrument, equipped with a Refractive Index (RI) detector and two PSS SDV 5 μm linear M columns. The eluent used was HPLC-grade THF, heated to 30 °C, and with a flow rate of 1.0 mL min^{-1}.

Differential Scanning Calorimetry (DSC): Carried out using a DSC 25 (TA Instruments). Samples were heated to 200 °C for 5 minutes, to remove thermal history, before heating and cooling from 30 °C to 200 °C at a rate of 10 °C min^{-1}. Glass transition temperatures (T_g) were recorded from the midpoint of the transition during the third heating curve.

Thermal Gravimetric Analysis: Carried out using a TGA/DSC 1 (Mettler-Toledo Ltd.) instrument. Samples were heated from 30 °C to 500 °C, under continuous N_2 flow, at a rate of 10 °C min^{-1}.

X-Ray Crystallography: Crystallographic data were collected, and structures solved, by Dr Ryan Kerr. Samples were isolated in a nitrogen filled glovebox and immersed in fluorinated oil. Crystalline samples were mounted on a MiTeGen Micromount and cooled to 150 K with dry nitrogen using an Oxford Cryosystem.[5] Data was collected using an Oxford Diffraction

Supernova diffractometer using Cu Kα (λ = 1.5417 Å) or Mo Kα (λ = 0.7107 Å) radiation. The resulting reflection data was processed with CrysAlis Pro.5 The crystal structures were solved using the SHELXT program and least-square refined using the SHELXL program within the Olex2 system suite.[6-8]

Elemental analysis was carried out by London Metropolitan University Elemental Analysis Service.

Representative Procedures

Epoxide/Anhydride Copolymerization

Inside a nitrogen filled glovebox, the complex and stated epoxide and anhydride monomers were added to a dried vial, equipped with a magnetic stirrer bar, in the ratios specified (*e.g.* [**2**]:[PA]:[CHO] = 1:400:2000). The vial was sealed with a melamine-cap containing a Teflon inlay, and further sealed with first Parafilm M and then electrical insulation tape. This sealed vial was then heated to the stated temperature for the stated time. Aliquoting was performed by first cooling the polymerisation vial outside the glovebox in a cold-water bath, before removing ca. 10 μL of the polymerisation mixture with a syringe in the glovebox. The polymerisations were quenched by exposing the reaction mixture to air, followed by removal of volatiles. A ^{1}H NMR spectrum of the crude product was measured in $CDCl_3$. GPC samples were prepared by dissolving ca. 10 mg of the crude product in 1 mL HPLC grade THF and filtered before use. Polymers were purified by precipitation from methanol and dried under vacuum at 40 °C.

Synthesis of Complexes

Synthesis of $L_{van}Fe(OAc)$ (1)

Under inert conditions, $[Fe(OAc)_2]$ (0.25 g, 1.4 mmol) was added to a stirred solution of $[L_{van}H_2]$ (0.53 g, 1.4 mmol) in anhydrous THF (10 mL) at 25 °C. The solution was stirred for 2 hours, before being exposed to air and stirred at room temperature for 16 hours, resulting in precipitation of a purple powder. The precipitate was isolated *via* centrifugation and was subsequently washed sequentially with THF (1 x 10 mL), toluene (3 x 10 mL) and hexane (3 x 10 mL) before being dried under vacuum to give **1** as a purple powder (0.49 g, 1.0 mmol, 71%). X-ray diffraction quality crystals were grown from a saturated solution of **1** in THF, layered with hexane. **IR**: 406, 419, 455, 506, 556, 565, 592, 612, 619, 634, 688, 723, 733, 742, 859, 866, 908, 912, 944, 972, 1046, 1068, 1079, 1092, 1159, 1169, 1192, 1221, 1231, 1248, 1301, 1325, 1357, 1365, 1387, 1397, 1408, 1432, 1445, 1462, 1520, 1548, 1605, 1618, 2833, 2898, 2932, 2959, 3052 cm^{-1}. **Anal. Calc.** $C_{23}H_{27}FeN_2O_6$: C, 57.16; H, 5.63; N 5.80 %. Found: C, 57.14; H, 5.53; N 5.99 %.

Synthesis of $L_{van}FeK(OAc)_2$ (2)

Under inert conditions, KOAc (24 mg, 0.24 mmol) was added to a stirred solution of complex **1** (120 mg, 0.24 mmol) in anhydrous 2-methyl THF at room temperature and was stirred for 16 hours. Subsequently the solvent was removed under vacuum to give **2** as a purple powder (144 mg, 0.25 mmol, 99%). X-ray diffraction quality crystals were grown from a saturated solution of **2** in chloroform, layered with hexane. **IR**: 416, 425, 452, 493, 500, 510, 558, 596, 612, 638, 733, 781, 855, 928, 965, 1011, 1068, 1108, 1152, 1169, 1221, 1241, 1307, 1365, 1438, 1470, 1551, 1611, 2836, 2892, 2954, 3054 cm^{-1}. **Anal. Calc.** $C_{25}H_{30}FeKN_2O_8 \cdot H_2O$: C, 50.09; H, 5.38; N 4.67 %. Found: C, 50.21; H, 5.13; N 4.30 %.

Supplementary Data and Figures

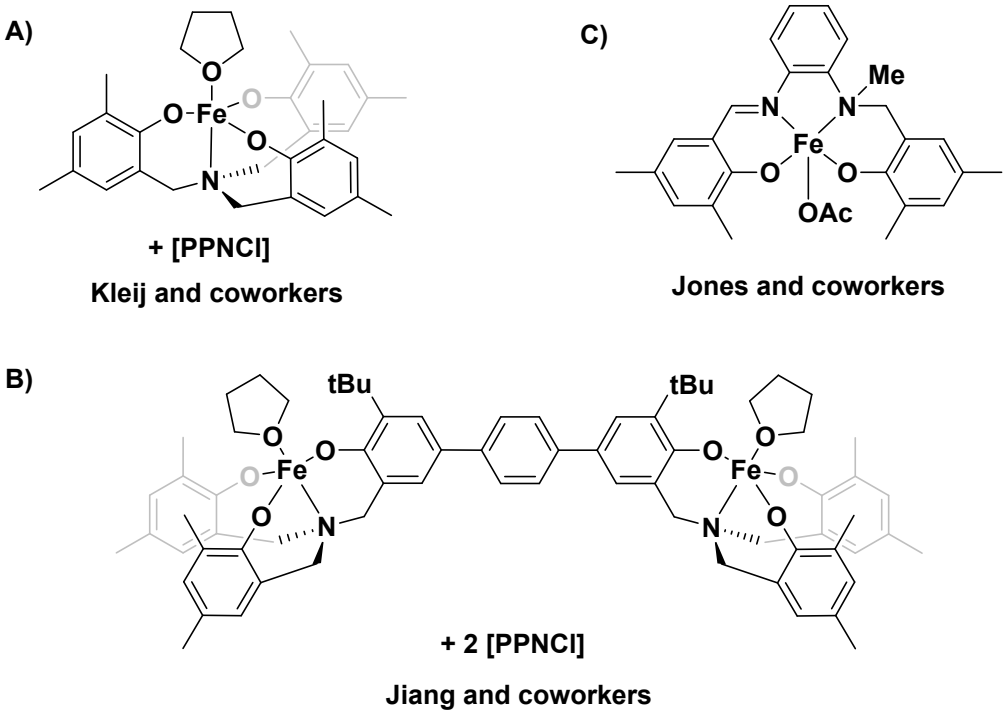

Figure S1. Structures of Fe(III)-based catalysts applied in epoxide/anhydride ROCOP.[9-11]

Table S1. Crystallographic collection and refinement data for complexes **1** and **2**.

Complex	**1**	**2**
Local Code	013rwfk22	008rwfk22
NAME	Fe	FeK
CCDC Number	2207318	2207317
Crystal Data		
Chemical formula	$C_{23}H_{27}FeN_2O_6$	$C_{25}H_{30}FeKN_2O_8$
M_r	483.31	581.46
Crystal system, space group	Monoclinic, $P2_1/c$	Triclinic, P^-1
a, *b*, *c* (Å)	9.0238 (2), 12.9234 (2), 19.4802 (3)	9.8770 (6), 12.1262 (9), 12.1406 (8)
a, b, g (°)	90, 96.797 (2), 90	66.668 (6), 83.456 (5), 83.448 (5)
V (Å^3)	2255.78 (7)	1322.68 (16)
Z	4	2
m (mm^{-1})	5.72	6.42
Crystal size (mm)	0.29 × 0.22 × 0.12	0.16 × 0.11 × 0.08
Data Collection		
Absorption correction	Gaussian *CrysAlis PRO* 1.171.40.53 (Rigaku Oxford Diffraction, 2019) Numerical absorption correction based on gaussian integration over a multifaceted crystal model Empirical absorption correction using spherical harmonics, implemented in SCALE3 ABSPACK scaling algorithm.	Multi-scan *CrysAlis PRO* 1.171.40.53 (Rigaku Oxford Diffraction, 2019) Empirical absorption correction using spherical harmonics, implemented in SCALE3 ABSPACK scaling algorithm.
T_{min}, T_{max}	0.452, 1.000	0.846, 1.000
No. of measured, independent and observed [$I > 2\sigma(I)$] reflections	52275, 4720, 4128	14130, 5480, 4834
R_{int}	0.062	0.030
$(\sin\theta/\lambda)_{max}$ (Å^{-1})	0.630	0.631
Refinement		
$R[F^2 > 2s(F^2)]$, $wR(F^2)$, *S*	0.031, 0.081, 1.03	0.036, 0.097, 1.03
No. of reflections	4720	5480
No. of parameters	294	340
$\Delta\rangle_{max}$, $\Delta\rangle_{min}$ (e Å^{-3})	0.32, -0.33	0.49, -0.31

Table S2. Selected Bond Lengths and Angles for Complex **1**

Bond	Length (Å)	Bond	Angle (°C)
Fe(1) – N(1)	2.0961(14)	O(2) – Fe(1) – O(5)	160.80(5)
Fe(1) – N(2)	2.0979(14)	O(3) – Fe(1) – N(1)	174.22(5)
Fe(1) – O(2)	1.9193(12)	N(2) – Fe(1) – O(6)	152.42(5)
Fe(1) – O(3)	1.9144(12)	O(5) – Fe(1) – O(6)	61.66(5)
Fe(1) – O(5)	2.1515(12)	O(5) – C(22) – O(6)	118.65(16)
Fe(1) – O(6)	2.0997(12)		
C(22) – O(5)	1.264(2)		
C(22) – O(6)	1.269(2)		

Table S3. Selected Bond Lengths and Angles for Complex **2**

Bond	Length (Å)	Bond	Angle (°C)
Fe(1) – K(1)	3.6177(6)	O(2) – Fe(1) – N(2)	171.51(6)
Fe(1) – N(1)	2.1266(17)	O(3) – Fe(1) – N(1)	177.46(6)
Fe(1) – N(2)	2.1394(16)	O(5) – Fe(1) – N(7)	168.79(6)
Fe(1) – O(2)	1.9615(13)	O(1) – K(1) – O(4)	172.09(5)
Fe(1) – O(3)	1.9393(14)	O(6a) – K(1) – O(8)	165.20(5)
Fe(1) – O(5)	1.9970(15)	O(5) – C(22) – O(6)	122.63(19)
Fe(1) – O(7)	2.0413(15)	O(7) – C(24) – O(8)	126.0(2)
K(1) – O(1)	2.6935(17)		
K(1) – O(2)	2.7539(16)		
K(1) – O(3)	2.7120(15)		
K(1) – O(4)	2.7303(17)		
K(1) – O(8)	2.7864(18)		
K(1) – O(6a)	2.7466(17)		
K(1) – O(8a)	2.7215(17)		
C(22) – (O5)	1.282(3)		
C(22) – O(6)	1.233(3)		
C(24) – O(7)	1.273(3)		
C(24) – O(8)	1.232(3)		

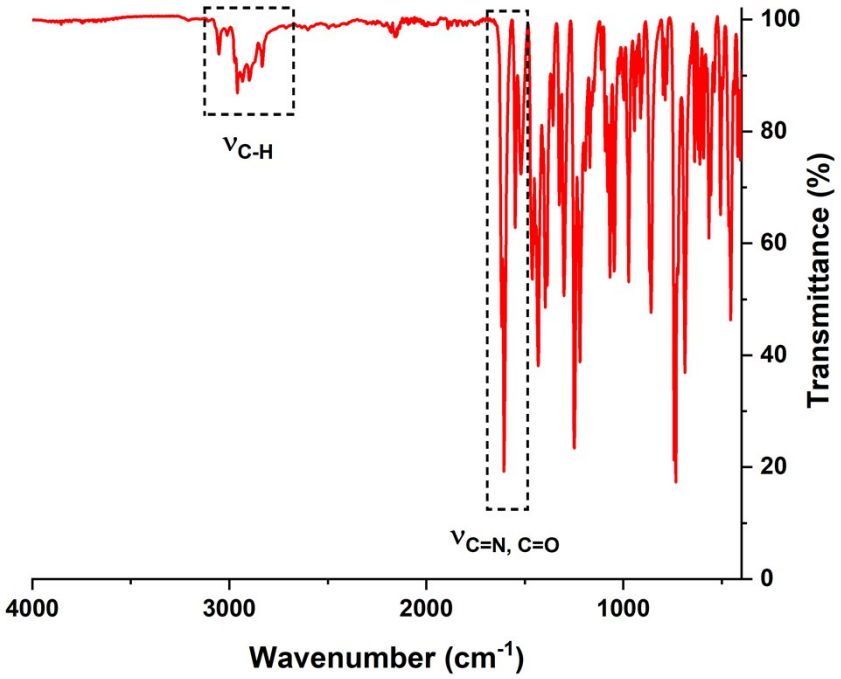

Figure S2. IR spectrum of complex **1**.

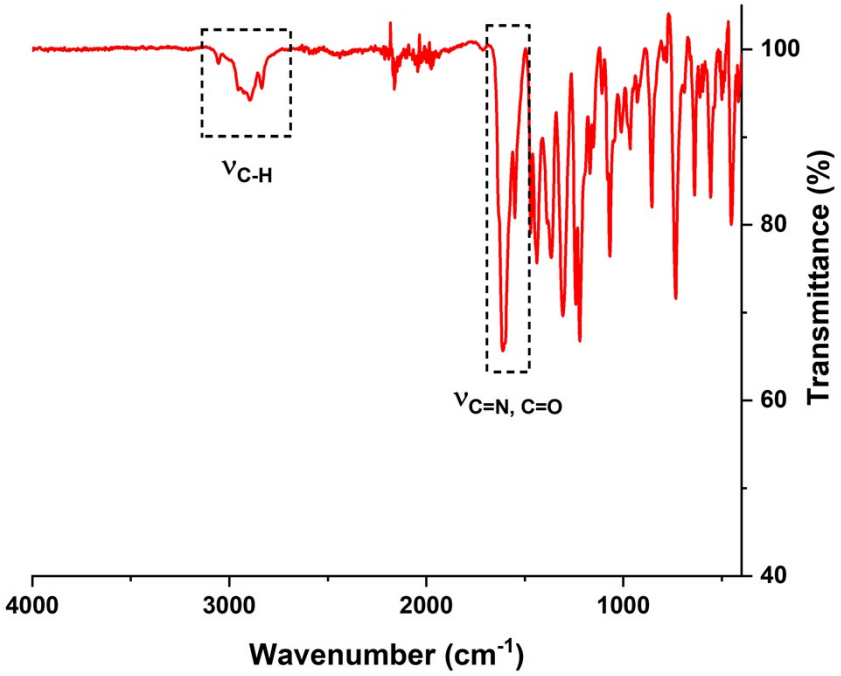

Figure S3. IR Spectrum of complex **2**.

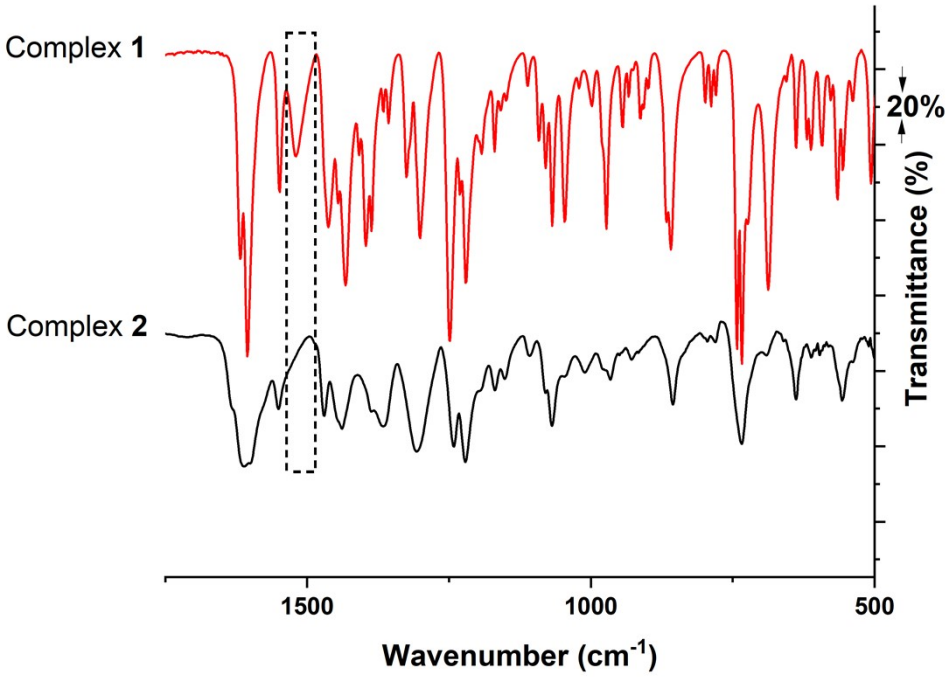

Figure S4. Overlay of IR spectra of complexes **1** and **2** (1750 – 500 cm^{-1}). Highlighted region shows disappearance of a stretch assigned to ν_{asymm}(C=O) in complex **1**, consistent with a shift in acetate binding mode from κ^2 to a ferrate structure. Full assignment of spectra is complicated by significant number of ligand-associated absorptions, including C=N stretches.

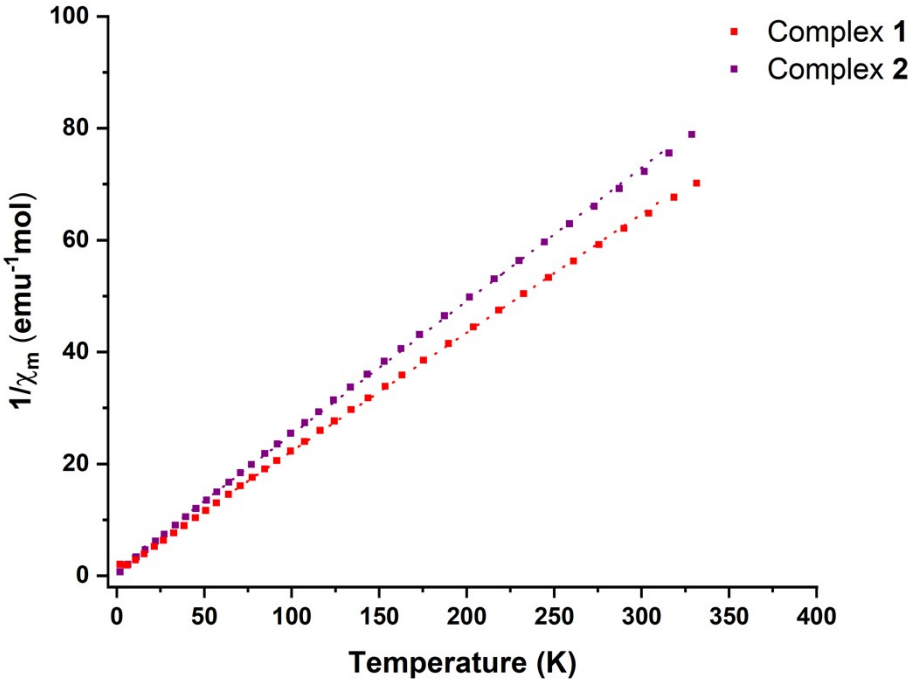

Figure S5. Plot of χmol^{-1} *vs*. temperature for complexes **1** and **2** obtained *via* SQUID magnetometry.

Table S4. Magnetometry data for complexes **1** and **2**.

Entry	Complex	C[a] (emu K mol^{-1})	θ[b] (K)	μ_{eff}[c]	S[d]	μ_{SO}[e]
1	**1** (Fe)	4.74	-5.38	6.10	5/2	5.92
2	**2** (FeK)	4.12	-4.62	5.69	5/2	5.92

[a] Curie constant is extracted from a plot of χ_{mol}^{-1} *vs*. temperature for each complex (Figure S5). From a linear fit of the data, $\chi_{mol}{}^{-1} = \alpha T + \beta,\ C = 1/\alpha$. [b] Weiss constant is extracted from a plot of χ_{mol}^{-1} *vs*. temperature for each complex (Figure S5). From a linear fit of the data, $\chi_{mol}{}^{-1} = \alpha T + \beta,\ \theta = x$ intercept. [c] Experimentally determined effective magnetic moment; $\mu_{eff} = 2.828\sqrt{\chi_m T}$ where $\chi_m = \frac{C}{T-\theta}$, T = 300 K. [d] Total spin quantum number, assuming high spin M(III) complexes. [e] Theoretical magnetic moment calculated from spin angular momentum only; $\mu_{so} = 2\sqrt{S(S+1)}$, which assumes complete quenching of *d* orbital angular momentum.

Table S5. Aliquot data corresponding to Table 1.[a]

Entry	Catalyst	[Cat]:[PA]	Temp (°C)	Time (min)	PA Conv.[b] (%)	TON[c]	$M_{n,\ GPC}$[c] (kg mol^{-1})	$M_{n,\ Th}$[d] (kg mol^{-1})	$M_{n,\ Th.\ Adj.}$[e] (kg mol^{-1})
1	**1**	400	100	120	36	144 ± 3	7.5	-	-
2[f]	**2**	400	100	15	72	288 ± 5	11.8	35.4	10.1
3[g]	**2**	400	100	15	73	292 ± 5	9.0	35.9	10.1
4	**2**	400	120	8	78	312 ± 5	10.8	38.3	10.9
5	**2**	400	140	5	>99	400 ± 7	14.0	49.2	14.1
6	**2**	1000	100	60	95	950 ± 16	19.1	116.9	16.1
7	**2**	2000	100	120	88	1760 ± 30	15.5	216.5	16.0
8	**2**	4000	100	360	94	3760 ± 63	17.8	462.5	17.8
9	**2**	4000	140	60	75	3200 ± 54	14.1	393.6	15.1

[a] General conditions: [Cat]:[PA]:[CHO] = 1:x:y where x is given in table and x:y = 1:5 (e.g Entry 1; [2]:[PA]:[CHO] = 1:400:2000). [b] Conversion of PA. Determined by ^{1}H NMR spectroscopy comparison of integrals corresponding to PA (8.10 – 7.85 ppm) and PCHPE (7.65 – 7.30 ppm). [c] Turnover number (TON) = number of moles of anhydride consumed/number of moles of catalyst. [c] Determined by gel permeation chromatography (GPC) in THF at 30 °C, using narrow dispersity polystyrene standards. [d] Theoretical molar mass. Determined by (TON*M_n(PCHPE repeat unit)/2. [e] Theoretical molar mass accounting for residual CTA. Following previously reported methodology, an intrinsic (residual) CTA ratio of $[CTA]_{residual}$:[PA]:[CHO] = 5:400:2000 is applied in calculation.[12] [f] Time taken between 3 and 18 minutes to account for induction period observed. GPC data presented from 18 minute aliquot. [g] Catalyst exposed to air for one week before reaction. Lower M_n attributed to water present in catalyst.

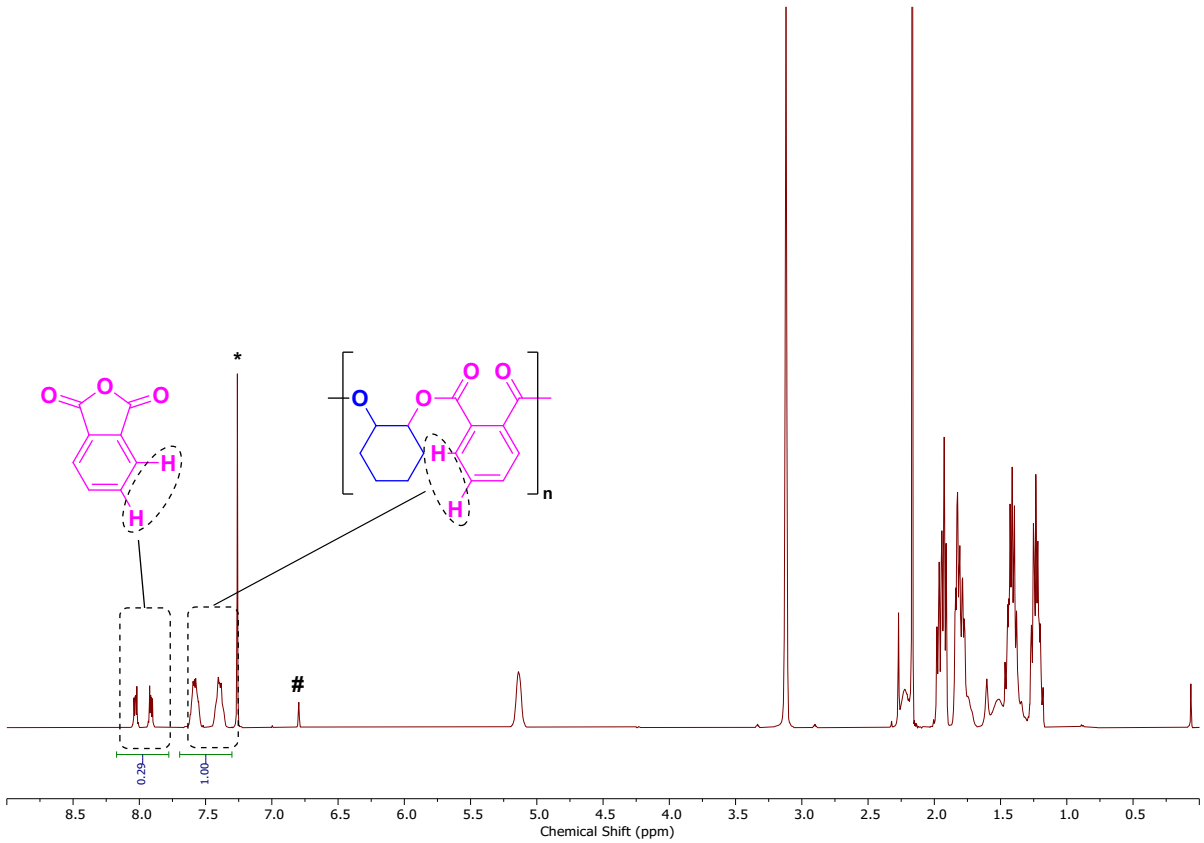

Figure S6. ^{1}H NMR spectrum (400 MHz, $CDCl_3$(*), 298 K) of ROCOP using CHO and PA. Mesitylene internal standard (#). Conversion of PA(%) = ((∫7.65-7.30 ppm)/(∫8.10-7.30 ppm))*100.

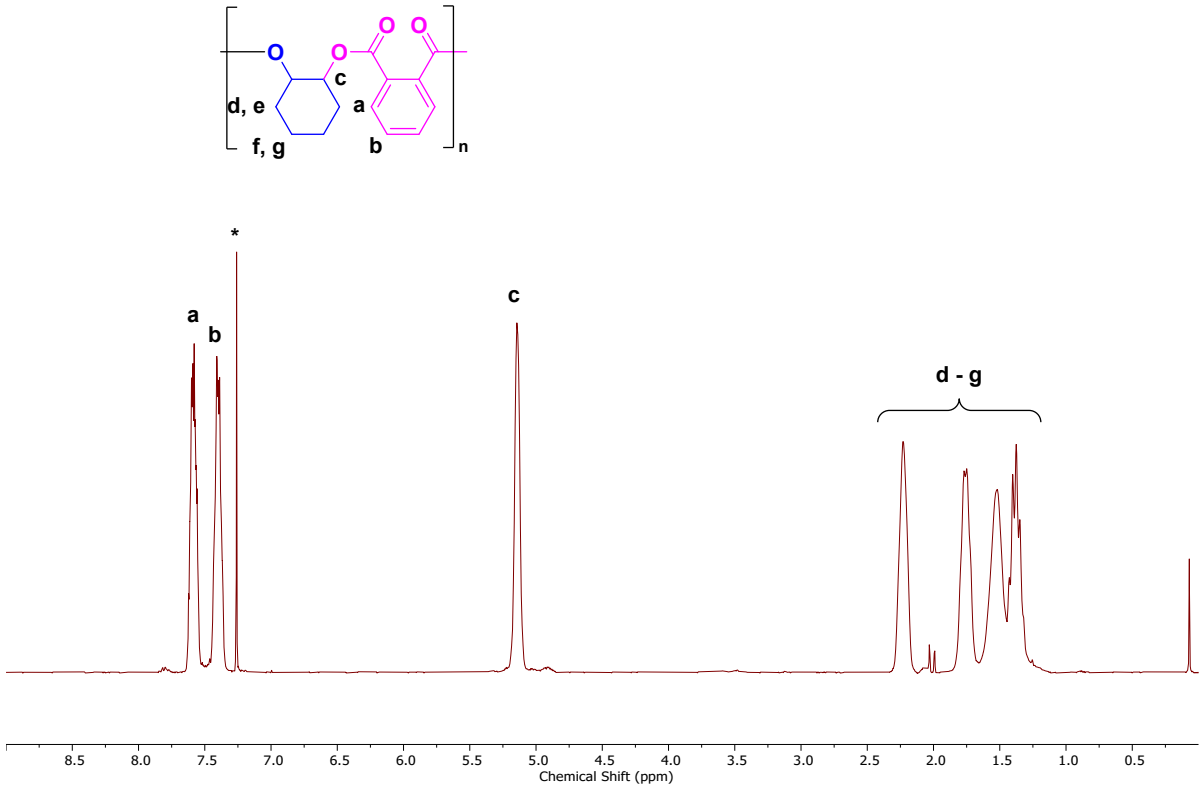

Figure S7. ^{1}H NMR spectrum (400 MHz, $CDCl_3$(*), 298 K) of pure polyester (poly(cyclohexene oxide-alt-phthalic anhydride).

Table S6. Data from the monitoring of bio-derived epoxide/anhydride ROCOP. [a]

Entry	Monomers	Time (h)	Temp.	Conv.[b] (%)	PE Select.[c] (%)	TOF[d] (h^{-1})	$M_{n,\ GPC}$[e]	Đ[f]
1	TCA/CHO	2	100	73	>99	146	10.3	1.23
2	CA/CHO	2	100	53	>99	106	7.0	1.23
3	FA/CHO	2	100	74	>99	148	10.5	1.15
4	PA/MO	10	100	89	>99	36	11.9	1.10
5	PA/LO	18	140	99	>99	22	5.0	1.23

[a] General conditions: [**2**]:[Anhydride]:[Epoxide] = 1:400:2000, T given in Table. [b] Conversion of Anhydride. Determined by ^{1}H NMR spectroscopy by comparison of integrals corresponding to monomer and polymer. [c] Selectivity for polyester (PE) over polyether. Determined by ^{1}H NMR spectroscopy by comparison of integrals corresponding to PE and polyether (3.5 – 3.0 ppm). [d] Turnover frequency (TOF) = TON/time (hours). Turnover number (TON) = number of moles of anhydride consumed/number of moles of catalyst. [e] Determined by gel permeation chromatography (GPC) in THF at 30 °C, using narrow dispersity polystyrene standards to calibrate the instrument. [f] Dispersity = M_w/M_n, determined by GPC in THF at 30 °C.

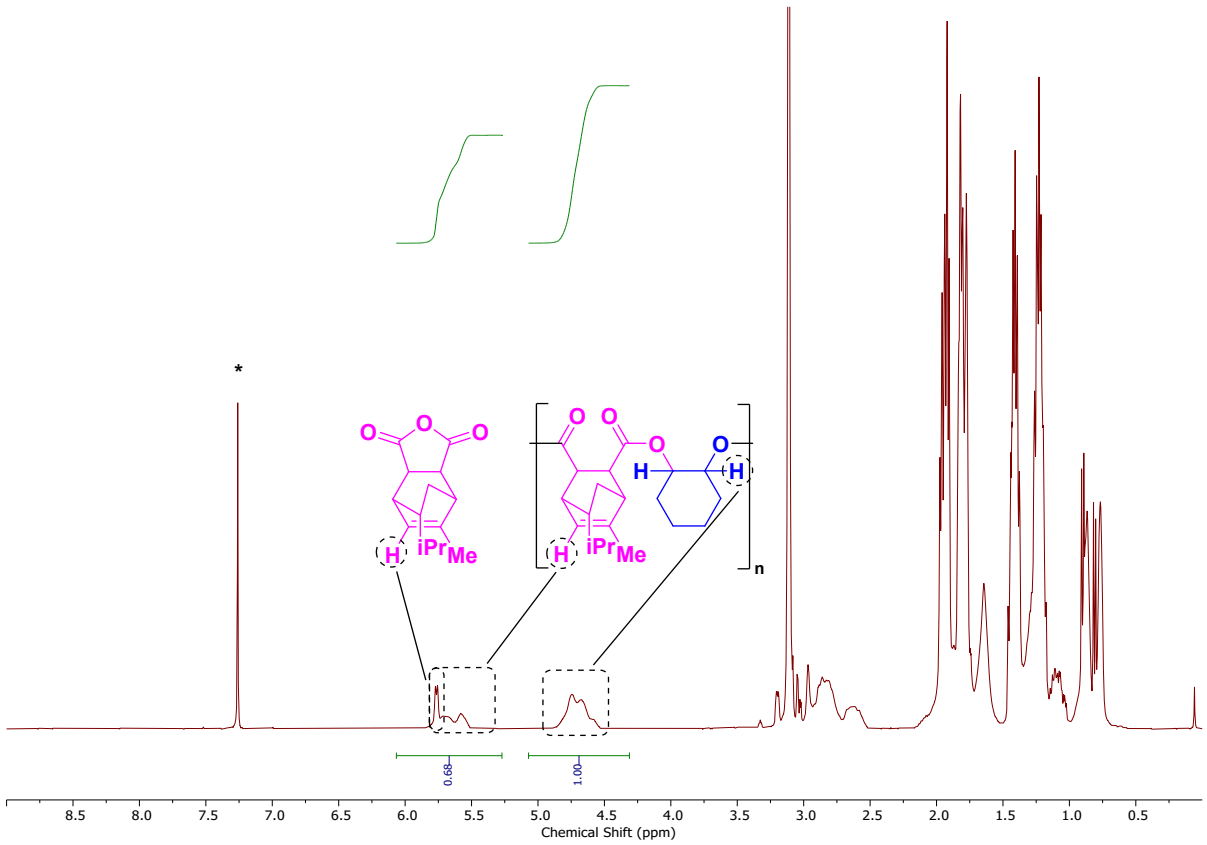

Figure S8. ^{1}H NMR spectrum (400 MHz, $CDCl_3$(*), 298 K) of ROCOP of CHO and TCA. Highlighted integrals used to calculate conversion.[13]

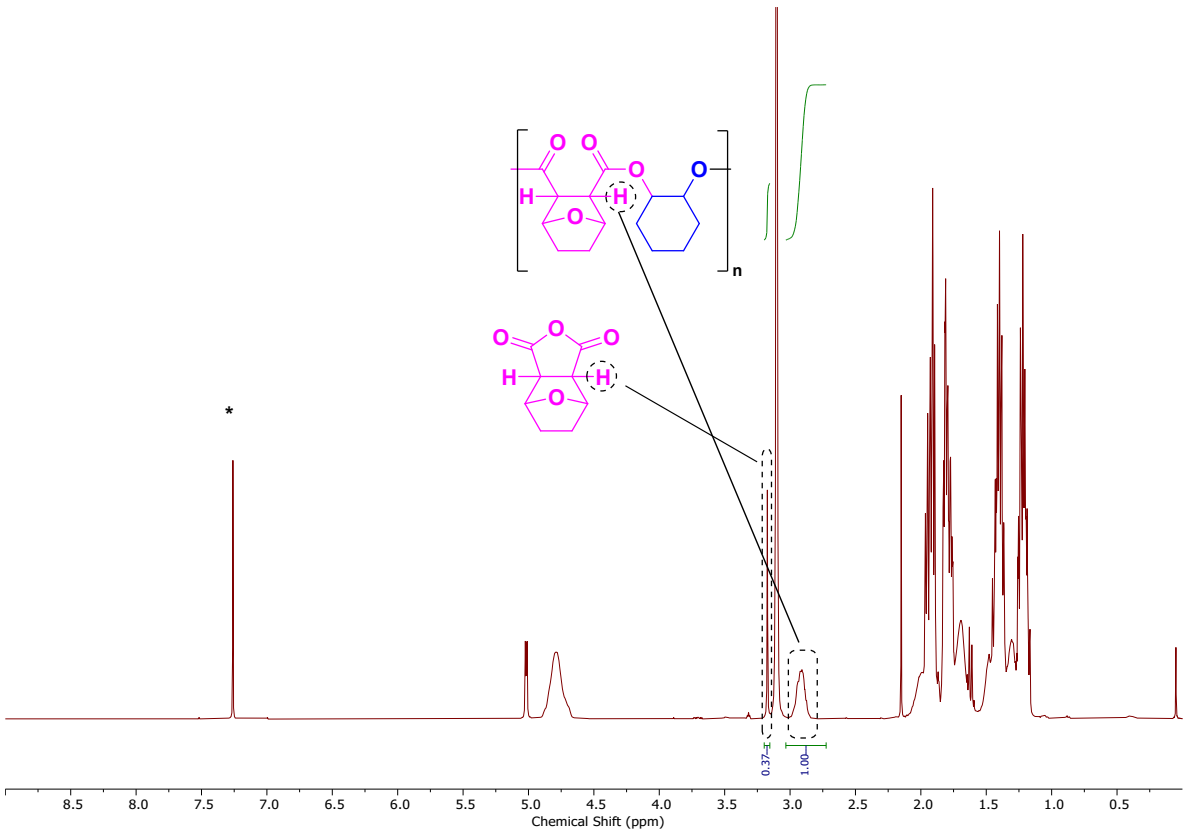

Figure S9. ^{1}H NMR spectrum (400 MHz, $CDCl_3$(*), 298 K) of ROCOP of CHO and FA. Highlighted integrals used to calculate conversion.

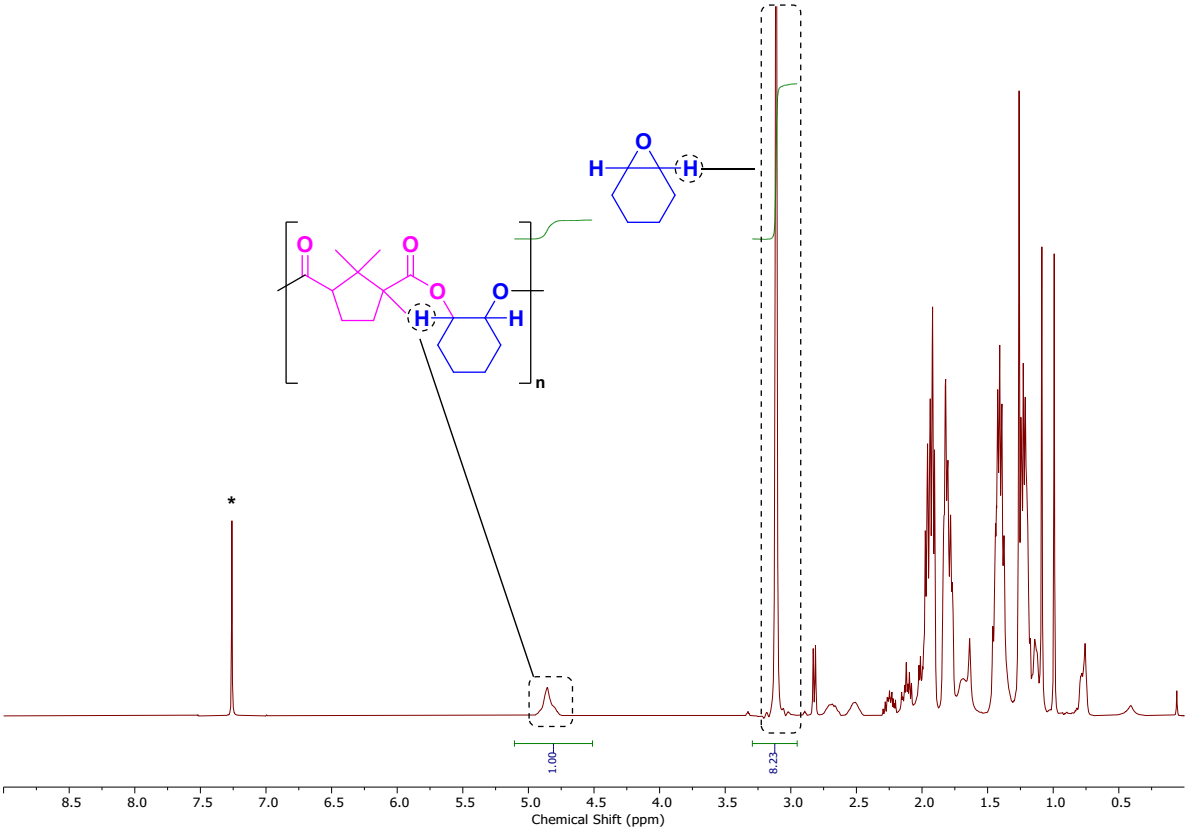

Figure S10. ^{1}H NMR spectrum (400 MHz, $CDCl_3$(*), 298 K) of ROCOP of CHO and CA. Highlighted integrals used to calculate conversion. *N.b.* that excess CHO is applied; full conversion of CA equates to 20 % CHO conversion.

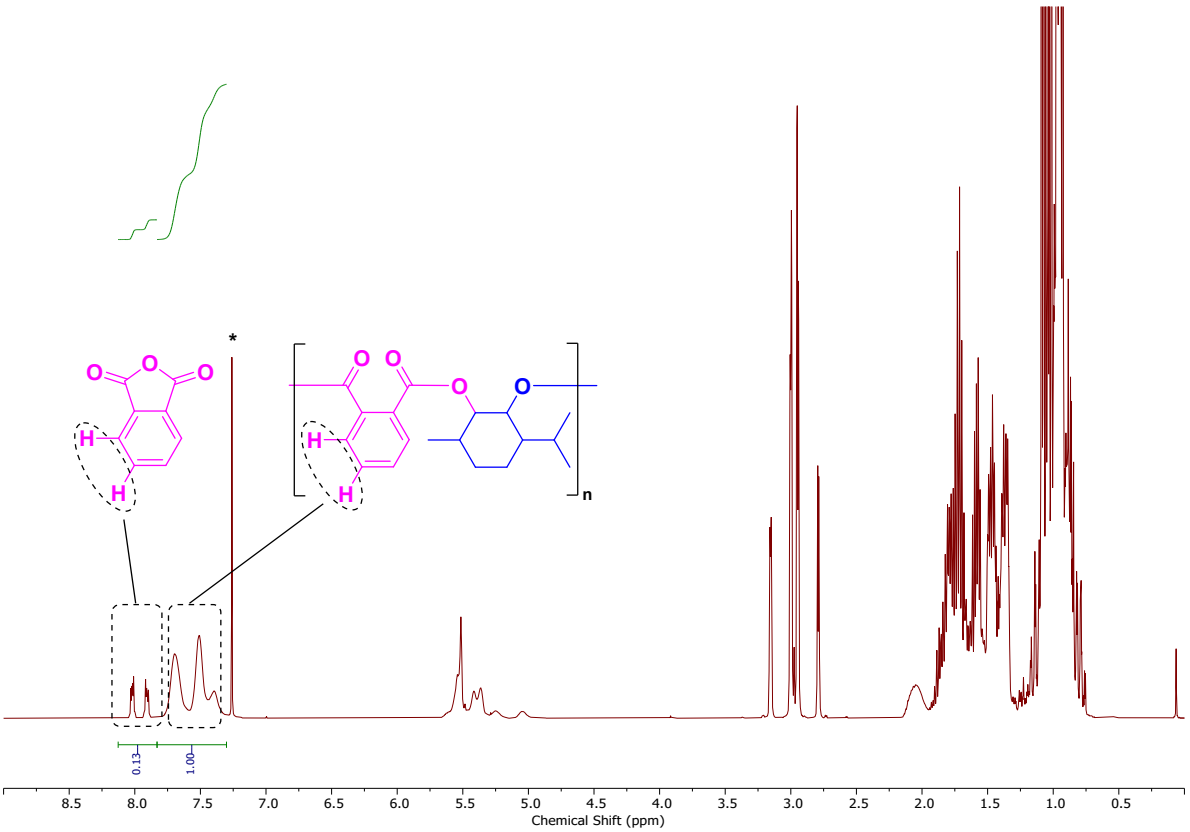

Figure S11. ^{1}H NMR spectrum (400 MHz, $CDCl_3$(*), 298 K) of ROCOP of MO and PA. Highlighted integrals used to calculate conversion.

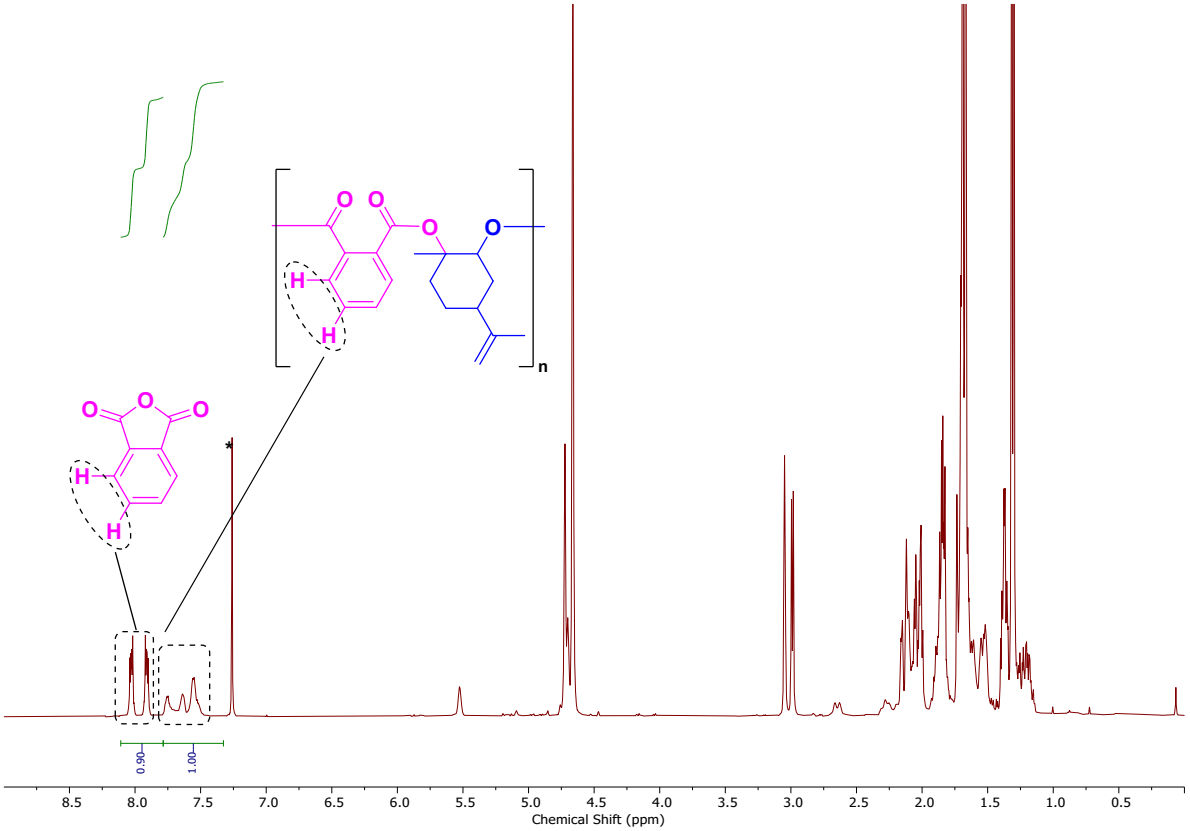

Figure S12. ^{1}H NMR spectrum (400 MHz, $CDCl_3$(*), 298 K) of ROCOP of LO and PA. Highlighted integrals used to calculate conversion. 10 hour timepoint used to illustrate PA integrals.

Table S7. Data for polyesters at full anhydride conversion. [a]

Entry	Monomers	Time (h)	Temp.	$M_{n,\,GPC}$[b]	Đ[c]	T_g[d] (°C)	$T_{d,5\%}$[e] (°C)
1	PA/CHO	0.42	100	15.4	1.07	136	304
2	TCA/CHO	4	100	14.6	1.23	156	327
3	CA/CHO	5	100	15.6	1.23	133	360
4	FA/CHO	4	100	13.1	1.18	167	309
5	PA/MO	12	100	13.2	1.12	177	294
6	PA/LO	18	140	5.0	1.23	112	253

[a] General conditions: [**2**]:[Anhydride]:[Epoxide] = 1:400:2000, T given in Table; all reactions at >99% conversion. [b] Determined by gel permeation chromatography (GPC) in THF at 30 °C, using narrow dispersity polystyrene standards. [c] Dispersity = M_w/M_n, determined by GPC in THF at 30 °C. [d] Determined by DSC, see Figure 4. [e] Determined by TGA, see Figure S15.

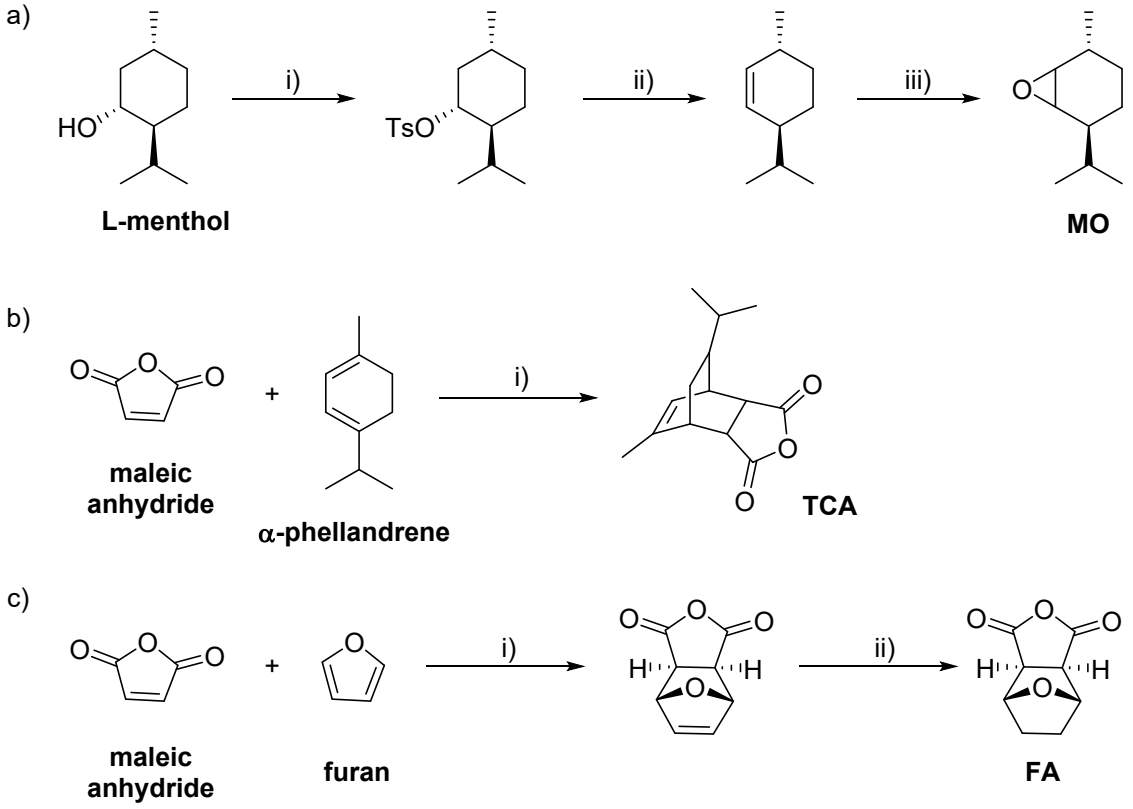

Figure S13. Bio-based syntheses of MO, TCA and FA. LO,[14] CHO,[15] PA[16] and CA[17] are commercially available but also have bio-based syntheses. a) i) TsCl, pyridine, 24 h, RT. ii) KOtBu, DMSO, 3h, 60 °C. iii) mCPBA, DCM, 8h, 0 °C then RT, 16 h. b) i) Acetone, 40 °C, 1 h. c) i) neat furan, 15 °C, 3 h ii) H_2 (1 atm) Pd/C (2 wt%), THF, RT, 16 h.

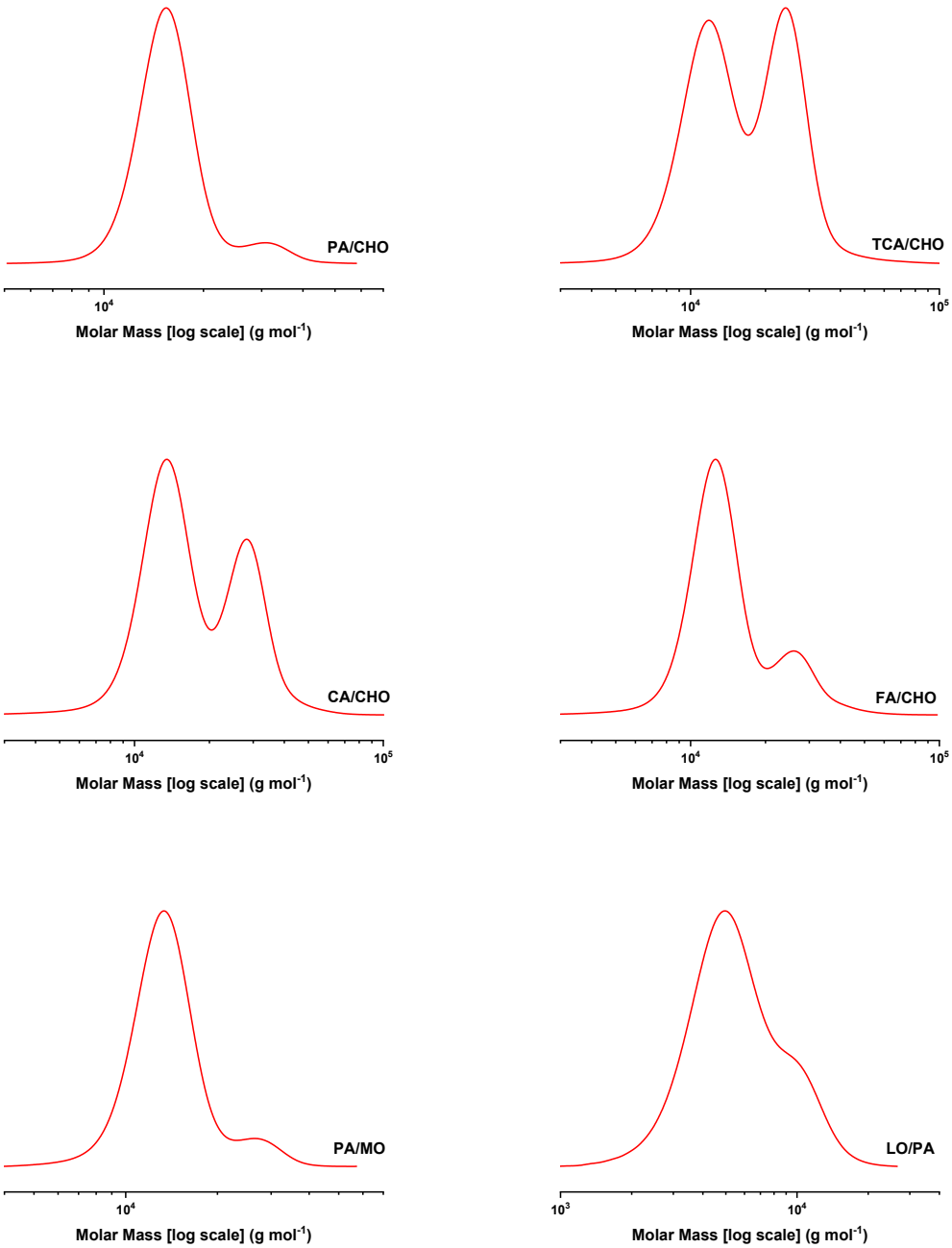

Figure S14. GPC traces for purified polymers corresponding to Table S7, Entries 1 - 6. *N.b.* some of the traces are bimodal as any trace water or acid results in formation of difunctional initiators which polymerize at the same rate as chains initiated from the catalyst derived acetate groups.[18] These phenomena are very commonly observed for epoxide/anhydride ROCOP catalysts.

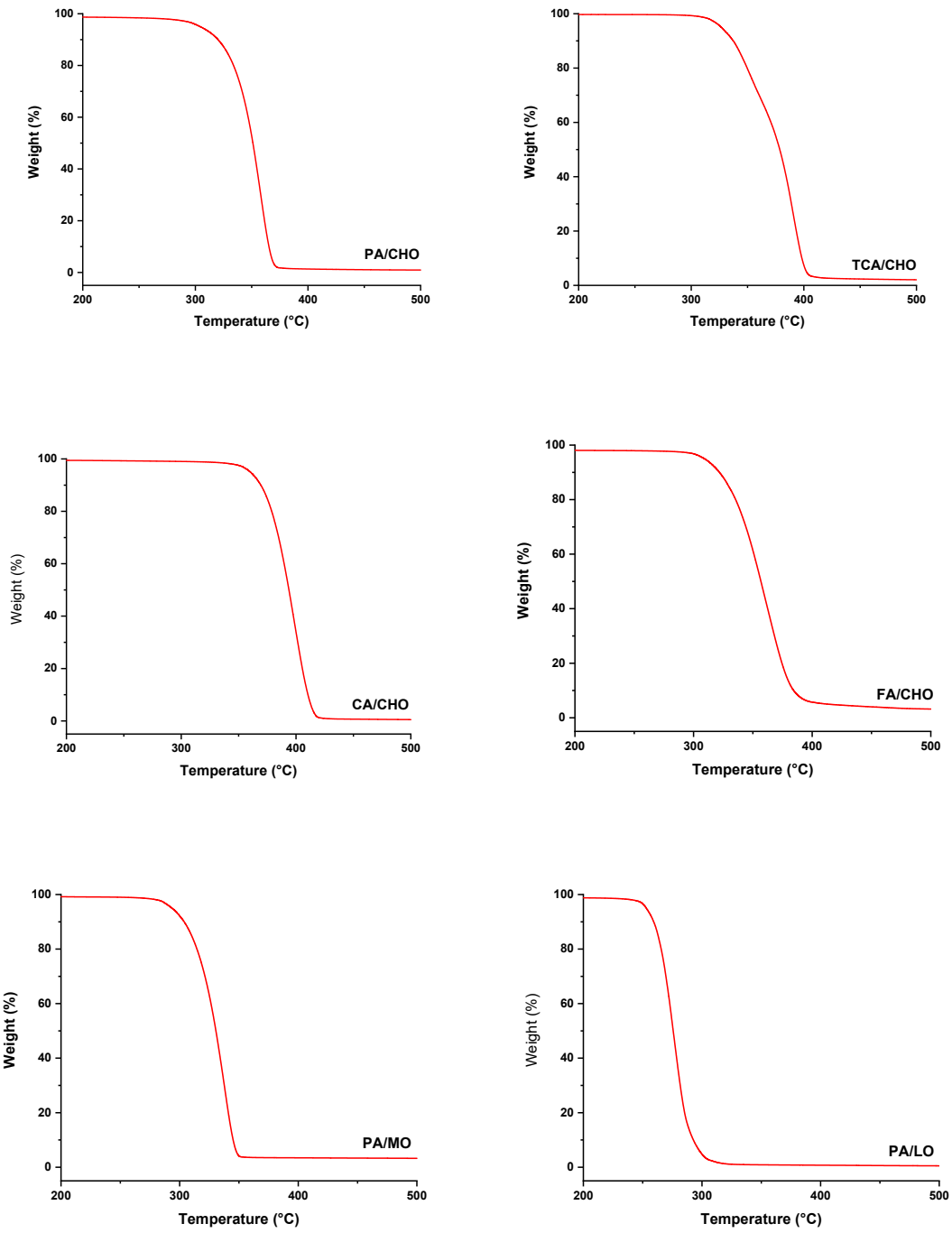

Figure S15. TGA Traces for purified polymers corresponding to Table S7, Entries 1 - 6.

References for SI

1. A. Wambach, S. Agarwal and A. Greiner, *ACS Sustainable Chem. Eng.*, 2020, **8**, 14690-14693.
2. D. Dakshinamoorthy, A. K. Weinstock, K. Damodaran, D. F. Iwig and R. T. Mathers, *ChemSusChem*, 2014, **7**, 2923-2929.
3. S. Thiyagarajan, H. C. Genuino, M. Śliwa, J. C. van der Waal, E. de Jong, J. van Haveren, B. M. Weckhuysen, P. C. A. Bruijnincx and D. S. van Es, *ChemSusChem*, 2015, **8**, 3052-3056.
4. A. Thevenon, J. A. Garden, A. J. P. White and C. K. Williams, *Inorg. Chem.*, 2015, **54**, 11906-11915.
5. J. Cosier and A. M. Glazer, *J. Appl. Cryst.*, 1986, **19**, 105-107.
6. G. M. Sheldrick, *Acta Cryst.*, 2015, **C71**, 3-8.
7. a) SHELXTL v5.1, Bruker AXS, Madison, WI, 1998 b) Sheldrick, G. M., *Acta Cryst.*, 2015, **A71**, 3-8.
8. O. V. Dolomanov, L. J. Bourhis, R. J. Gildea, J. A. K. Howard and H. Puschmann, *J. Appl. Cryst.*, 2009, **42**, 339-341.
9. A. Brandolese and A. W. Kleij, *Acc. Chem. Res.*, 2022, **55**, 1634-1645.
10. O. J. Driscoll, J. A. Stewart, P. McKeown and M. D. Jones, *Macromolecules*, 2021, **54**, 8443-8452.
11. Z. Shi, Q. Z. Jiang, Z. Z. Song, Z. H. Wang and C. L. Gao, *Polym. Chem.*, 2018, **9**, 4733-4743.
12. W. T. Diment and C. K. Williams, *Chem. Sci.*, 2022.
13. W. T. Diment, G. L. Gregory, R. W. F. Kerr, A. Phanopoulos, A. Buchard and C. K. Williams, *ACS Catal.*, 2021, **11**, 12532-12542.
14. T. T. D. Chen, L. P. Carrodeguas, G. S. Sulley, G. L. Gregory and C. K. Williams, *Angew. Chem. Int. Ed.*, 2020, **59**, 23450-23455.
15. M. Winkler, C. Romain, M. A. R. Meier and C. K. Williams, *Green Chem.*, 2015, **17**, 300-306.
16. S. Giarola, C. Romain, C. K. Williams, J. P. Hallett and N. Shah, *Chem. Eng. Res. Des*, 2016, **107**, 181-194.
17. M. G. Moloney, D. R. Paul, R. M. Thompson and E. Wright, *Tetrahedron Asymmetry*, 1996, **7**, 2551-2562.
18. D. J. Darensbourg, *Green Chem.*, 2019, **21**, 2214-2223.